ORIGINAL ARTICLE

Porosity formation and its effect on the properties of hybrid laser welded Al alloy joints

Shaohua Yan[1] · Zhongyin Zhu[2] · Chuanping Ma[2] · Qing-H. Qin[3] · Hui Chen[2] · Y. N. Fu[4]

Abstract

Laser-arc welding is increasingly applied for joining aluminum alloys. A critical issue in laser-arc welding Al alloys is the existence of pores which can significantly influence the in-service properties of the welded joints. How to control the porosity, therefore, is of importance in both academic and industrial worlds. In this paper, effects of welding parameters on the degree of porosity in welded joints were investigated. The distribution and size of pores were characterized by X-ray and synchrotron radiation X-ray detection methodology. It was found that the porosity was successfully controlled by adjusting welding parameters. Specifically, the macropores were reduced dramatically by increasing arc currents and decreasing laser powers. Macropore-free joints were obtained with some welding parameters. The mechanism of controlling macropores was presented. Moreover, the results from mechanical testing showed that the pores did not obviously influence the mechanical properties for low percentage of porosity in the range of near 0 to 4%, but decreased the fatigue strength of the joints. EBSD results illustrated that the grain size of the fusion zone was about 74 ± 58 μm, and no obvious texture was found within the fusion zone.

1 Introduction

Laser-arc welding has seen increasing usage in manufacturing modern industrial structures of aluminum alloys, since this advanced welding technology features with high welding speed, deep penetration, and stable welding process [1]. However, problems still exist in hybrid laser welding Al

✉ Shaohua Yan
   shaohua.yan@anu.edu.au

✉ Qing-H. Qin
   qinghua.qin@anu.edu.au

✉ Hui Chen
   xnrpt@163.com

1   School of Science, Harbin Institute of Technology, Shenzhen 518055, China

2   School of Materials Science and Engineering, Southwest Jiaotong University, Chengdu 610031, China

3   Research School of Eletrical, Energy and Materials Engineering, College of Engineering and Computer Science, The Australian National University, Acton, ACT 2601, Australia

4   Shanghai Synchrotron Radiation Facility, Shanghai Institute of Applied Physics, Shanghai 201204, China

alloys, of which the handicapped one is the porosity in the welded joints. Aluminum alloys have high thermal conductivity and dramatic differences in the solubility of hydrogen during solidification [2], which lead aluminum alloys to forming pores with high possibility. The generation of pores in laser-arc welding can be attributed to two reasons: (a) the instability of the keyhole that can cause macroscale pores [3], and (b) the trapped shielding gas or hydrogen that results in microscale pores [4]. Macroscale pores can reduce the statistic and dynamic strength of the joints [5], whereas microscale pores can influence the dynamic strength [6, 7]. Thus, how to prevent the formation of pores in laser-arc welding Al alloy is a challenging and primary task in both academic and industrial welding communities.

Since collapse of keyholes in hybrid laser welding is the key mechanism for the formation of macropores [8, 9], significant efforts have been made to stabilize the keyhole by adjusting the welding parameters, including laser power, arc power, welding speed, the distance between two heat sources etc. For example, Zhang et al. [10] studied the effect of the welding parameters, which covered arc welding current, laser power, distance between laser and arc, defocusing amount, and welding speed, on the porosity of laser-arc welded AA6082
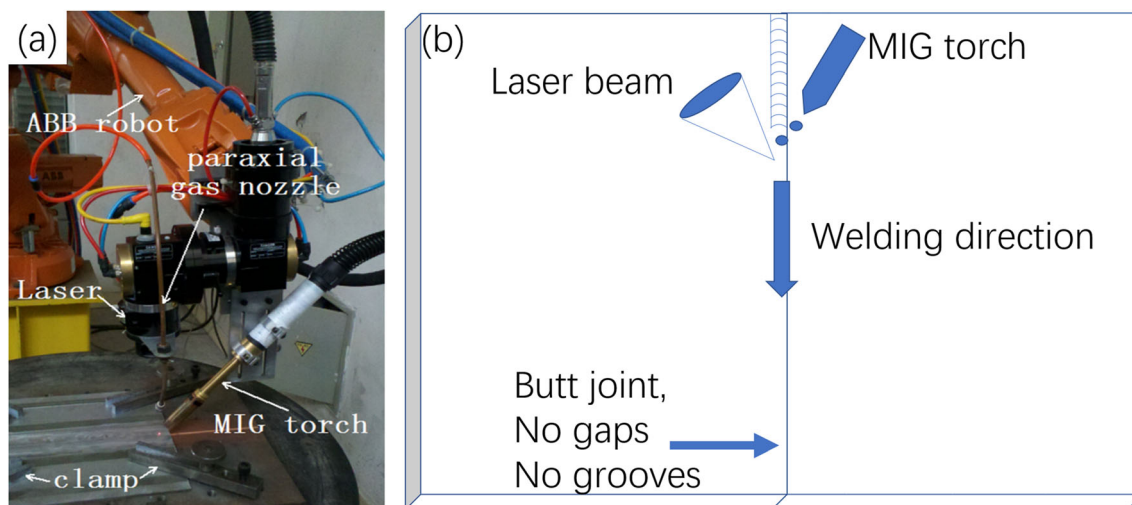
Fig. 1 **a** Hybrid laser welding system used in this study [1], and **b** schematic of the butt joint

joints. They reported that the porosity could be decreased in several ways, such as increasing the arc welding current and laser powers and reducing the welding speed. Bunaziv et al. [5] examined the influence of the trailing torch arrangement and the shielding gas on the formation of pores in laser-arc welded AA5083 joints. A large number of macropores were observed when putting the MIG torch as the trailing heat source, whereas no effect of shielding gas was found on decreasing macropores. Seiji et al. [11] studied the influence of arc welding current on the porosity of hybrid laser welded AA5052 joints and found that increasing the arc current reduced the porosity in the weld. Leo et al. [12] claimed that the ratio of laser power to arc power controlled the formation of macropores. They reported that high laser power resulted in extensive Mg evaporation and as a result more pores were found in the fusion zone. The obtained joint, featuring high porosity and loss of Mg, was reported to have poor mechanical properties. Thus, decreasing the laser power was recommended to obtain sound welded joints. Similarly, Ola et al. [13] investigated the role of laser power, defocus, and distance between the laser and arc on the formation of pores in hybrid laser welding AA2024. They reported that pores increased significantly when applying high laser power. Contrary to the conclusion from Leo and Ola et al., Casalino et al. [14] reported that sound welded joints could be obtained by increasing laser power, as it could stabilize the welding process and help with obtaining structural and geometrical properties of joints.

Although extensive studies have been performed in investigating the formation of pores, the mechanism behind the hybrid laser welding is still under debate. Besides, current studies have involved too many welding parameters to obtain sound joints, which are

inconvenient and indirect for the researchers to find appropriate welding parameters. Furthermore, the ultimate purpose of achieving pore-free joints is to make the joints stronger (in terms of statistic strength) and more endurable (in-service life). Nevertheless, fewer effects have been paid to investigate the porosity-property relationship. In this paper, only two main welding parameters, laser power and arc currents, were considered for laser-arc welding 5-mm-thick AA60005 plates. The relationship between the porosity of the welded joints and welding parameters was investigated via X-ray and synchrotron radiation X-ray detecting method. Macropore-free joints were obtained under special welding parameters. Moreover, the microstructure and properties of the joints were also examined. The main aim of this paper is to provide useful guideline for reducing pores in laser-arc welding Al alloys.

Table 1   Welding parameters used in this study [16]

Welding parameters	Value range
Laser power (P_L)/kW	1.5–3
Arc current (I)/A	130–210
Welding speed (v)/m·min^{-1}	0.64–0.83
Defocusing distance (L_0)/mm	0
Distance between laser beam and filler wire (D_{LA})/mm	2
The angle of the laser beam to the welding direction/°	75
The angle of the MIG torch to the welding direction/°	56
Weld stick-out length/mm	12
Shielding gas flow rate/L·min^{-1}	25
Shielding gas	Argon (99.999%)

Fig. 2. Image from X-ray detection testing shows the morphology of pores and the welded joint
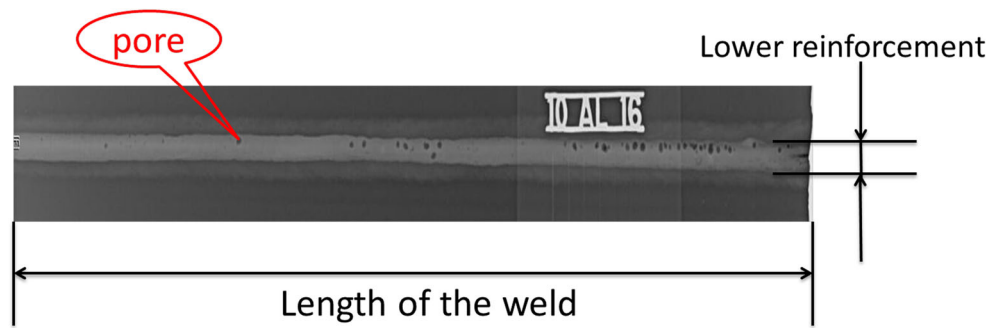
2 Experimental methods

2.1 Sample preparation

AA6005 plates with the dimension of 120 mm × 240 mm × 5 mm were joined via laser-MIG welding system as described in Refs. [1, 15]. The schematic of the welding system is shown in Fig. 1a; constant and variable welding parameters used in this study are shown in Table 1. The butt joint was made in this paper and no gaps and grooves were used in the welding, as illustrated in Fig. 1b. Welded joints under different welding parameters were examined to detect the porosity using a non-destructive X-ray detective system with the minimum resolution of 0.1 mm. The porosity percentage was calculated according to standard ISO-10042, as shown in the following equation:
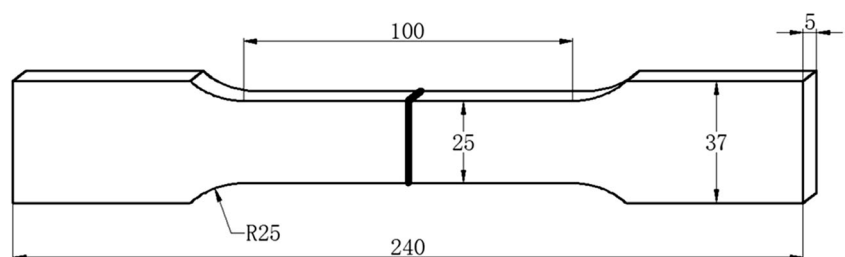
$$\text{Porosity percentage} = \frac{\sum_i^N Si}{Sp} \qquad (1)$$

where S_i is the area for each pore in the joint, and S_p is the projection area that is defined by the length and the width of lower reinforcement of the weld, as shown in Fig. 2. Samples for tensile testing were prepared according to the standard of ASTM B557-15, whose dimension is shown in Fig. 3. The tensile test was performed at the speed of 0.5 mm/min.

2.2 Synchrotron radiation X-ray

In order to obtain 3D images of internal pores in the laser-arc welded joint, synchrotron radiation X-ray method (SR-XRM) experiment was performed at the 13-W beam line (BL13W) in Shanghai. The chosen energy was 26 keV. The samples were cylindrical (3 mm in diameter) with no polishing on their surface. For each sample, 700~1400 2D slices were recorded on a 2048 × 2048 CCD camera developed at Shanghai Synchrotron Radiation Facility. These successive 2D slices were subsequently reconstructed using Amira software for 3D images. The resolution of synchrotron radiation is 0.32 μm.

2.3 Microstructure observation

To examine the microstructure in the cross-section of the welded joints, samples were polished using the procedure shown in Table 2. After polishing, a sample was etched using Keller's solution to observe the microstructure under optical microscope. A scanning electron microscope (SEM), Zeiss Ultraplus SEM, was used to do electron back scatter diffraction (EBSD) testing. The testing parameters were the same as those in Ref. [17]. The chemical composition of the matrix was measured by energy dispersive spectroscopy (EDS). The sample for the transmission electron microscope (TEM) examination of the fusion zone was prepared by an ion polishing method in a precision ion polishing system (PIPS).

2.4 Residual stress and modeling

Residual stress is known to affect the fatigue resistance of welded components. To know the distribution of residual stress, stress analyzer (PROTO, Canada) was applied to measure the residual stress in the hybrid laser welded AA6005 joints. The parameters for residual stress measurement were as follows: Cr-kα radiation, 20 kV, 4 mA, (222) diffraction plane, and 156.9° diffraction angle. The heat source model for

Fig. 3 Dimensions of the sample for tensile testing

Table 2 Procedure for grinding and polishing samples

	Step	Grinding paper/polishing cloth	Polishing solution	Sample speed (RPM)	Plate speed (RPM)	Force (lbf/N)	Time (min)
Grinding	1	400 Grit SiC paper	Water	300	300	22	5
	2	800 Grit SiC paper	Water	300	300	22	5
	3	1200 Grit SiC paper	Water	300	300	22	5
	4	2000 Grit SiC paper	Water	300	300	22	5
Polishing	1	Polishing cloth	6-μm polycrystalline diamond paste and glycol suspension	300	300	22	10
	2	Polishing cloth	3-μm polycrystalline diamond paste and glycol suspension	300	300	22	10
	3	polishing cloth	0.02-μm colloidal silica solution	150	150	13	60

All consumables were purchased from Allied High-Tech Products, Inc.

arc welding was defined by a double ellipsoid model, while the laser heat source was a conical heat source.

2.5 Fatigue test

Fatigue samples were machined from the welded joints with direction perpendicular to the welding direction, and the dimensions of the sample are shown in Fig. 4. Before the fatigue test, all the samples were visually inspected, and no macroscopic defects were observed. The fatigue tests were performed with tension-tension cyclic loadings at a stress ratio of $R = 0.1$. The frequencies ranged from 100 to 110 Hz. The fracture of the fatigue samples was observed by SEM in order to identify the sites of fatigue cracks and the propagation mechanism.

3 Results

3.1 Porosity distribution

Figure 5 shows the images of X-ray inspection for the joints under different welding parameters. With inappropriate joining parameters (i.e., $P_L = 3$ kW, $I = 130$ A), the size and number of pores are relatively large. This finding can be explained by the collapse of the keyhole during welding [18]. By adjusting the welding parameters, the size and density of the pores are reduced. More specifically, as illustrated in Fig. 6,

the porosity is reduced from 4% to near 0% when increasing the welding current from 130 to 210 A while decreasing the laser power from 3 to 1.3 kW. It can be seen from the results that a high-quality welded joint can be obtained by decreasing the laser power and increasing the current simultaneously. The optimized welding parameters to achieve sound welds from the experiments in this study are as follows: $P_L = 1.3$ kW, $I = 210$ A, $\nu = 0.63$ m min^{-1}.

The coarse pores at macroscale can be avoided by selecting appropriate welding parameters. However, complete avoidance of pores is beyond reality, as demonstrated in Fig. 7a which presents a SEM image of the fractured surface. The SEM image shows that micro-sized cavities exist in the fusion zone, which is due to the release of gas by the surface boiling or the protecting gas used in welding [4]. Limited by the resolution of X-ray detection, it is difficult to obtain the size and distribution of pores in the weld. Here we use high-resolution SR-XRM to detect the pore distribution. As shown in Fig. 7b, most pores are spherical-shaped. Unlike the previous reports from Refs. [19, 20], there are no differences in the upper and lower parts of the fusion zone regarding the pore size and density. To quantitatively analyze the pores in the fusion zone, the Schwartz-Saltykov analysis method in Ref. [21] was used to obtain the size and volume of pores. The results are shown in Fig. 7c, from which it can be seen that diameter of most pores is less than 150 μm, while only few pores have their diameters greater than 500 μm.

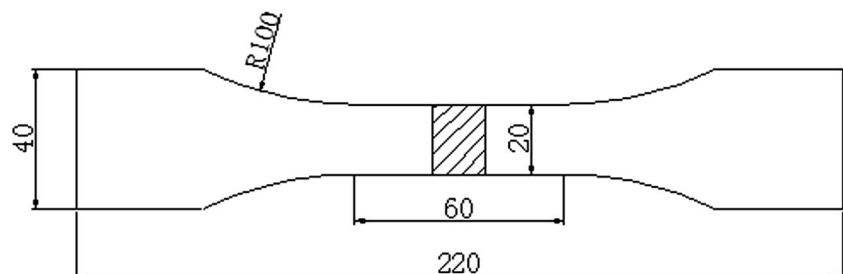**Fig. 4** Dimensions of samples for fatigue testing

Fig. 5 Distribution of pores in the welded joints under different welding parameters by X-ray detection method

P_L kW	I A	V m·min⁻¹	X-ray image
3	130		
2.5	130		
2.3	130	0.83	
2.2	130		
2	170		
1.8	160		
1.8	180		
1.5	180	0.64	
1.5	190		
1.3	210		

3.2 Microstructure and mechanical properties

The tensile strength and elongation of the laser-arc welded AA6005 joints are shown in Fig. 8a. For comparison, the strength of the base metal is also presented in Fig. 8a. The averaged strength of joints does not change very much,
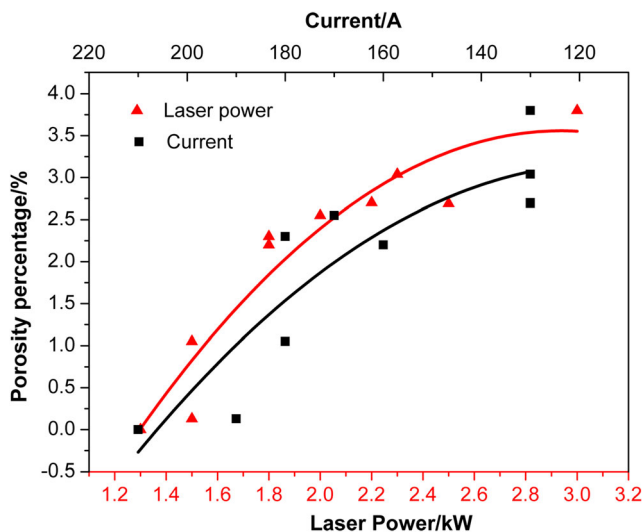

Fig. 6 Porosity under different laser powers and currents

ranging from 198 to 209 MPa. This indicates that the porosity does not affect the tensile strength in this research. It should be noted that the strength may be deteriorated when the porosity is higher [5], especially when the joint contains a large number of coarse pores. The largest strength is 206 MPa achieved under the welding parameters of P_L = 1.3 kW, I = 210 A, v = 0.63 m min⁻¹. But the strength of the joint is still lower than that of the base metal (276 MPa); the softening may be attributed to the evaporation of alloying elements [22]. The elongation of the joints is higher with decreasing porosity, as illustrated in Fig. 8b. The best elongation corresponds to the welded joint achieved under the optimized welding parameters.

Figure 9 shows the microstructure of the fusion zone in the welded joint under the optimal welding parameters. It can be seen from Fig. 9a–b that coarse phases distribute on the matrix. EDS was conducted to examine the chemical composition of the solid-solution area in the fusion zone, and the results show that Mg dominates the solid solution; this finding is similar to that in Ref. [17, 23]. Multiple-element (Cr–Si–Al) phases are found from the TEM results, as shown in Fig. 9c. Moreover, Mg_2Si may be found in hybrid laser welded AA6005 alloy joints as indicated in Ref. [24]. The EBSD results (Fig. 9d) show that equiaxed grains present in the
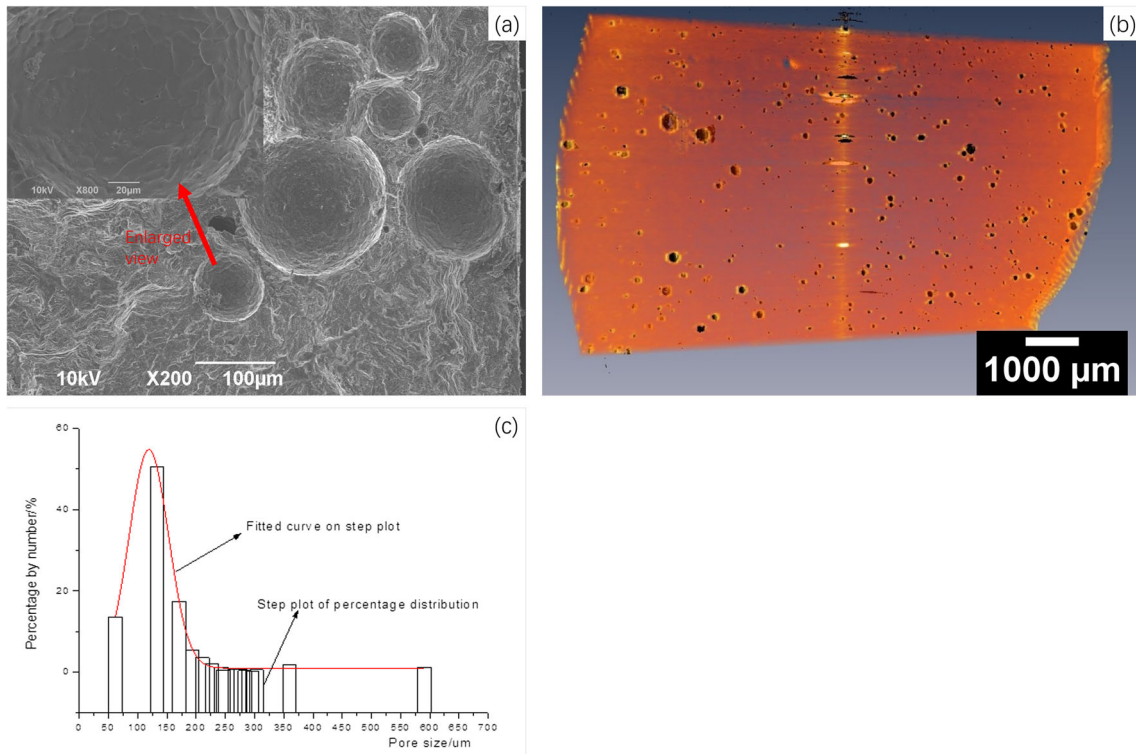
Fig. 7 **a** Micropores in the welded joints, **b** 3D distribution of the micropores obtained by synchrotron radiation X-ray detection, and **c** size and volume curves of micropores in the welded joints

fusion zone, and no obvious texture is found. According to the intercept measuring method, the grain size in the fusion zone is about 74 ± 58 μm; the finding is similar to that in Ref. [17].

3.3 Residual stress

Residual stress obtained from experiments and simulation is shown in Fig. 10a, from which it can be seen that tensile stress locates near the fusion zone of the joints, and compressive stress exists in the HAZ and BM. The simulation of the residual stress (see Fig. 10b) demonstrates a symmetric distribution of stress with the tensile stress in the fusion zone and compressive stress in HAZ and BM. The temperature during the welding is shown in Fig. 11. Highest temperature (540 °C) is in the center of the welding pool, and the temperature decreases with the distance increasing from the center of the welding pool.

3.4 Fatigue strength

As demonstrated in Fig. 8a, the porosity of the joints in this work shows little influence on the average tensile strength of
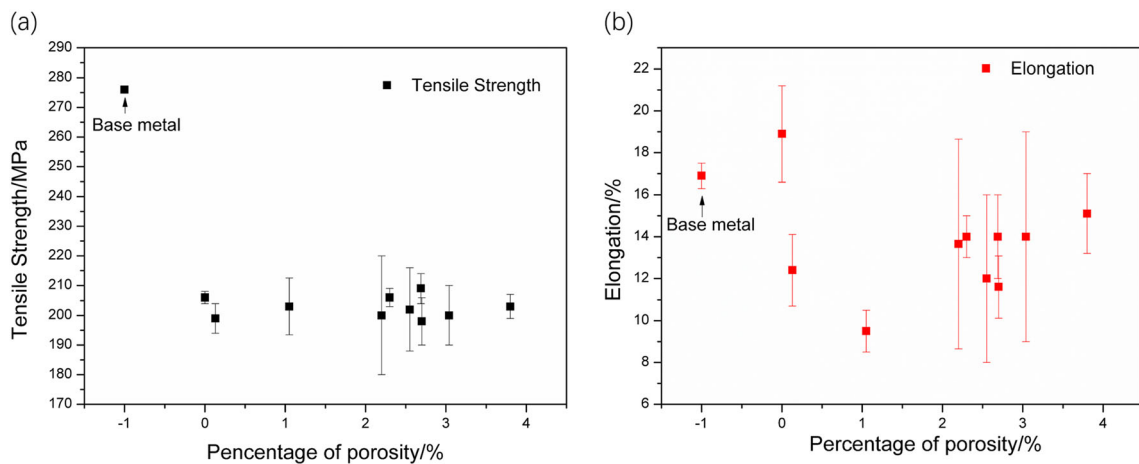

Fig. 8 The effect of porosity on the tensile strength (**a**), and elongation of hybrid welded AAA6005 joint (**b**)
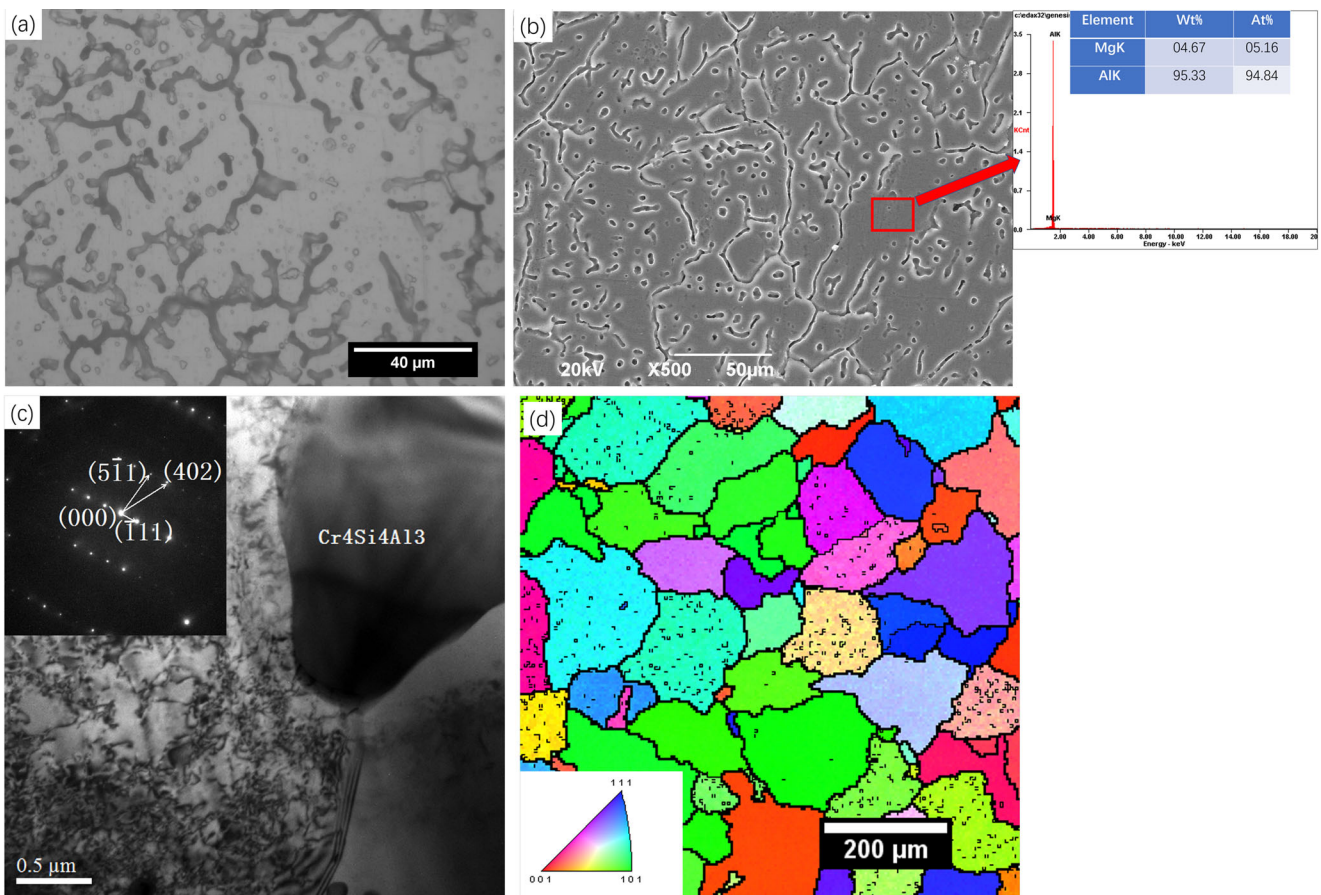
Fig. 9 Microstructure of the fusion zone, **a** the optical image, **b** SEM image and EDS results, **c** TEM image for the precipitate in the fusion zone, and **d** EBSD results

laser-arc welded AA6005 joints. However, what role can these pores play when the joints are under dynamic loading? In this section, the fatigue life of the welded joints was studied. Two types of joints were considered, one was with the upper and lower reinforcement (referred as un-grinded joints) whereas the other was grinded to have flat surface. The un-grinded joints, having upper and lower reinforcement, leads to stress concentration due to the notch effect. As a result, the fatigue life of the as-welded joint is largely reduced, as shown in Fig. 12; the fatigue strength at $N = 10^7$ cycles is only 50 MPa.

The grinded joint, as illustrated in Fig. 12, has increased fatigue strength at $N = 10^7$ cycles, which is 115 MPa. The improvement is mainly due to the increase of the toe's radius, which results in the decrease of the stress concentration.
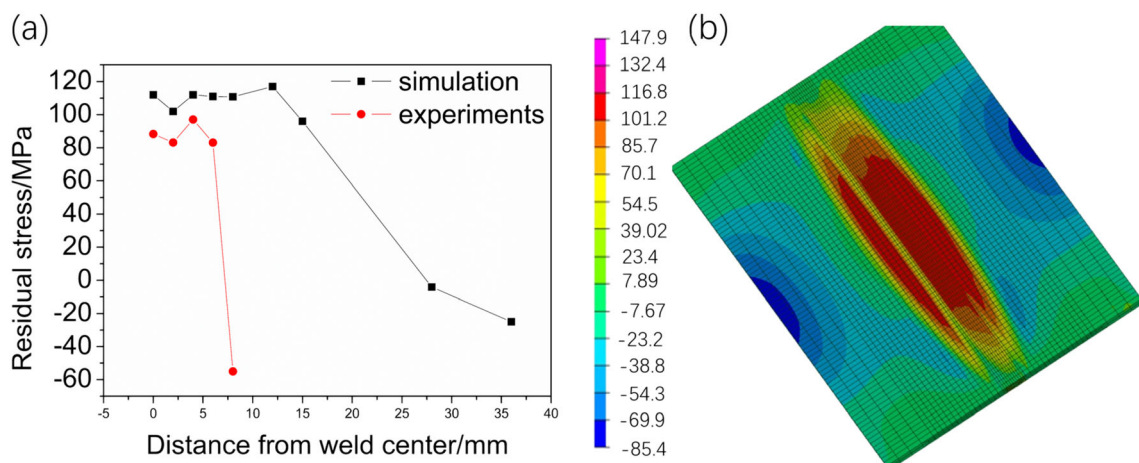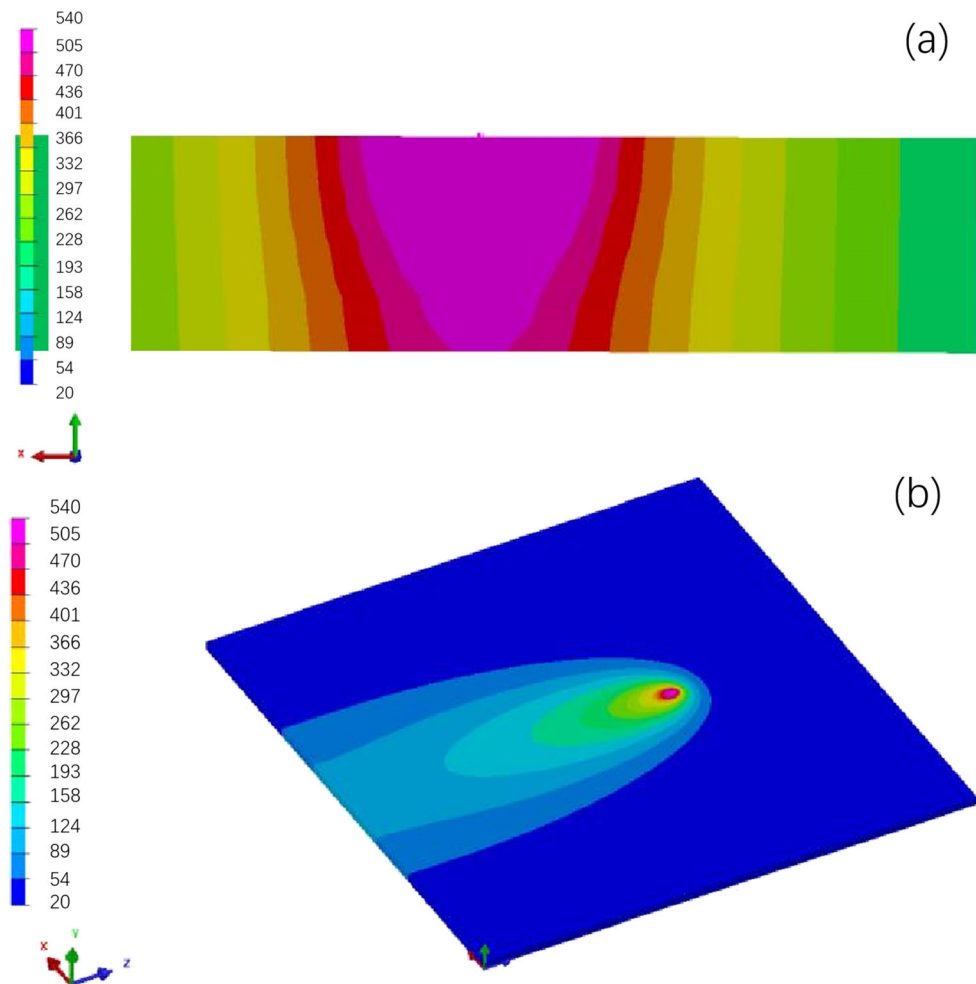

Fig. 10 **a** Residual stress of the joint from X-ray diffraction experiments and simulation, and **b** simulated distribution of residual stress

Fig. 11 **a** Cross-sectional view of the temperature distribution, **b** and temperature distribution during the welding

(a)

(b)

However, compared to the base metal, the fatigue strength of the grinded joint is still smaller. The fatigue limit of the base metal at 10^7 cycles is 140 MPa. The softening in fatigue strength is possibly caused by the defect inside the joint. As shown in Fig. 13a, b, places with pores close to the sample's surface are preferable sites for the initiation of fatigue cracks. However, in the base metal, no such big pores exist; the fatigue strength is thus higher.

4 Discussion

4.1 Effect of welding parameters on the formation of porosity

The results displayed in Section 3.1 (see Fig. 6) show that the porosity in the hybrid laser welding can be well controlled by contracting the laser power and increasing the arc current. This improvement can be explained from two aspects, the stability of the keyhole and the movement of the bubble.

As illustrated in Fig. 5, the pores in the joints are large at millimeter scale when the laser power is high. By decreasing

the laser power and increasing the arc current at the same time, the size and density of pores are decreasing. The trend, increasing laser power causing greater porosity, is consistent with other experimental and numerical results from Refs.
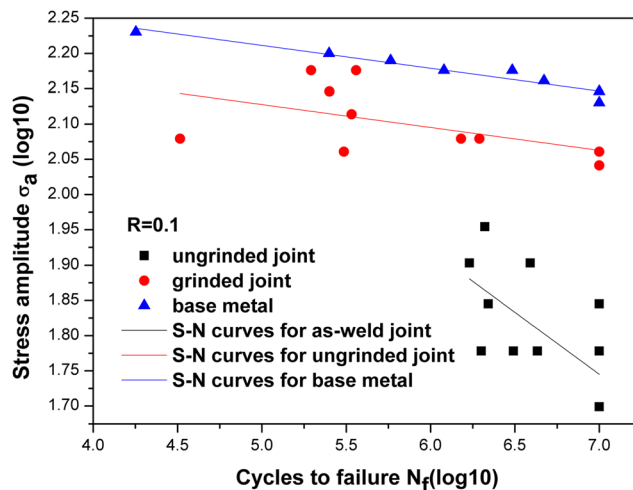

Fig. 12 Fatigue LgS-LgN curves for hybrid welded AA6005 joints and the base metal
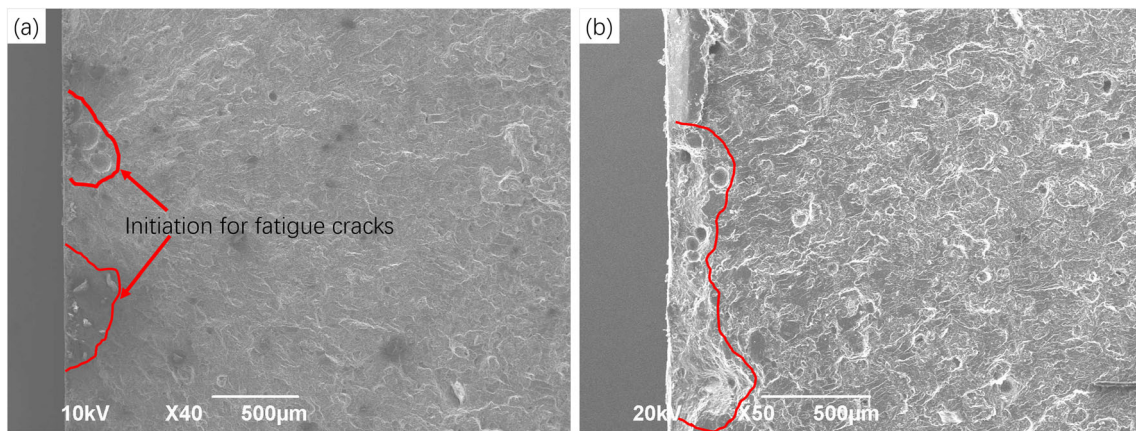
Fig. 13 SEM images of fatigue crack propagation sites which had extensive pores, **a** σ_S = 130 MPa, without reinforcement, N_f = 3.4E6, and **b** σ_S = 150 MPa, without reinforcement, N_f = 1.9E6

[25, 26]. The formation of large pores is mainly caused by the instability of the keyhole during welding. As shown in Fig. 14a, according to Ref. [27], the balance of the keyhole is maintained by:

$$P_r + P_v = P_s + P_h \tag{2}$$

where P_r is the recoil pressure, P_v is the vapor pressure, P_s is the pressure from surface tension effects, and P_h is the hydrostatic pressure. The two terms on the left-hand side of Eq. (2) tend to open the keyhole, whereas the two terms on right-hand side drive the keyhole to collapse. It is worth to note that the keyhole is in fluctuating status in welding. In other words, the balance of the keyhole is not in reality during welding since the environment around the keyhole always changes depending on the welding parameters. The instability or collapse of the keyhole would trap the gas to form bubbles during welding, leading to macroscale porosities in the joints, as indicated in Refs. [28, 29]. If the laser power is higher, the height-to-width radius of the keyhole is greater [19], as shown in Fig. 14b, which could lead to higher surface tension pressure. Since the external pressure ($P_s + P_h$) is bigger, the

keyhole is then easy to collapse to trap the bubble, resulting in pores in the welds. Furthermore, large height of the keyhole makes the bubble escaping from the keyhole more difficult at such rapid solidification time. When lowering the laser power and increasing the arc current, as shown in Fig. 14c, the keyhole and the welding pool becomes bigger [30], the height-to-width radius of the keyhole is smaller [31], and the welding pool is shallower which can shorten the floating distance of bubbles. Therefore, the possibility of collapsing keyhole is smaller. Besides, increasing arc current slows down the solidification rate of the welding pool, which, consequently, provides more time for floating of bubbles.

Although the coarse pores can be largely reduced by stabilizing the keyhole, micro-sized pores can still be observed, as demonstrated in Fig. 7a. The hydrogen-induced pores are formed because of the change of the solubility of hydrogen atom in aluminum at liquid and solid state [2]. In the liquid-state aluminum, the solubility of hydrogen is about 0.69 ml/100 g, whereas the value can be reduced to 0.036 ml/100 g in the solid-state aluminum. Therefore, the concentration of hydrogen dissolving in the molten pool will decrease rapidly in
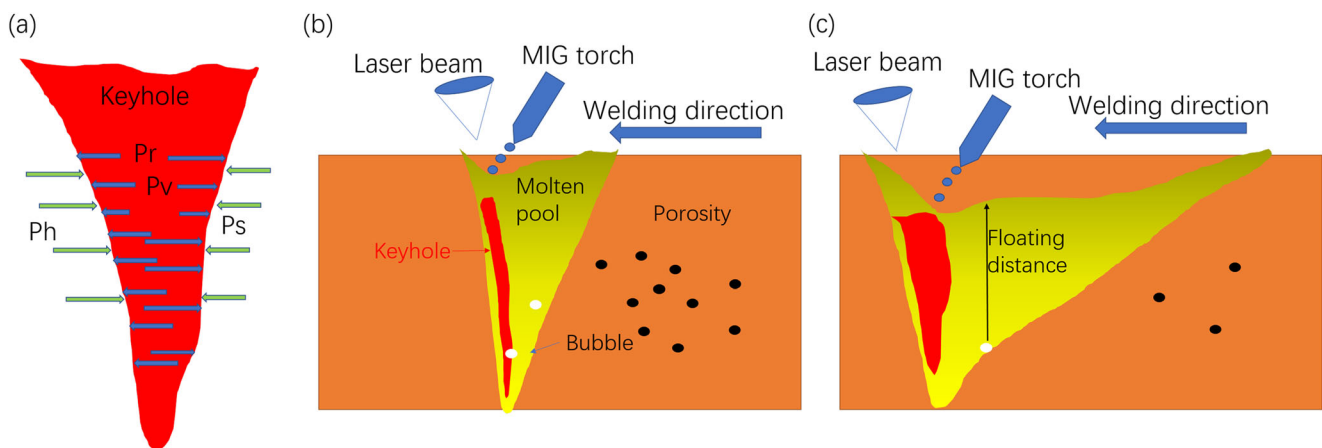

Fig. 14 Schematic drawing of **a** internal and external pressure of a keyhole, **b** the keyhole and molten pool under welding parameters of low arc currents and high laser power, and **c** the keyhole and molten pool under welding parameters of high arc currents and low laser power
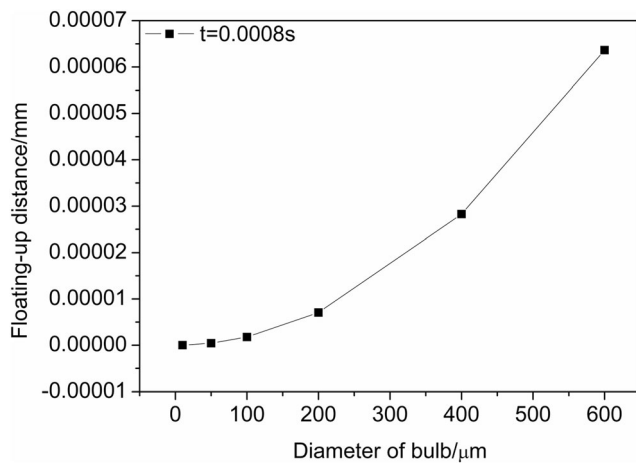
Fig. 15 Floating-up distance for bubbles with various diameters; the floating time is 8 ms.

the solidification processing, leading to the generation of hydrogen gas bubble. The gas bubble would float up after its generation. The floating-up rate of the bubble can be expressed as [32]:

$$\nu_f = \frac{2(\rho_1 - \rho_2)gr^2}{9\eta} \qquad (3)$$

where ρ_1 and ρ_2 are the density of the molten metal and the gas bubble, respectively. r is the radius of the bubble, g is the gravity acceleration, and η is the viscosity coefficient of the molten metal. Referring to Ref. [10], the parameters in Eq. (3) are taking as $\rho_1 = 4420$ kg m^{-3}, $\rho_2 = 1.784$ kg m^{-3}, and $\eta = 0.005$ kg s^{-1} cm^{-1}. Given that the typical time for solidification is about 8 ms [32], the calculated floating-up distance for different-diameter bubble is shown in Fig. 15. The bubbles with the diameter less than 600 μm can only go up 0.00006 mm, as illustrated in Fig. 15. This finding indicated that these bubbles would be trapped during the solidification process, and the micropores cannot be eliminated.

4.2 Effect of pores on the properties of joints

The tensile testing results, shown in Fig. 8a, show that low percentage of pores has no influence on the tensile strength of the welded joints, a finding which is consistent with the work of Wu et al. [21], who built a model to qualify the effect of pores on the yield strength of hybrid laser welded AA7075 alloy joints and found that the strength was not affected by pores. However, our work is contrast to that of Bunaziv et al. [5] who reported that pores can reduce the strength of welded AA5085 joints. In their work, the porosity of the joint was up to 50%, which was much greater than the present case (the maximum value being 4% only). It is reasonable that, for the case of Bunaziv et al. [5], the tensile strength of welded joints would be much worse since the effective load-bearing area in the fusion zone was largely reduced due to the large number of

pores. The elongation of the welded joint is influenced by the porosity, as demonstrated in Fig. 8b. Since the cracks can initiate from the defects, such as pores and voids, high porosity can lead to greater loss of ductility [12].

It is found from the SEM observation (Fig. 13) that the fatigue cracks initiate from the pores close to the sample's surface, suggesting that the pores have an influence on the fatigue strength of welded joints. The pore-induced softening in the fatigue resistance of welded joints has been reported previously. For example, Yan et al. [17] investigated the effect of microstructure and pores on the fatigue strength of AA6061 joints. They found that pores could significantly reduce the fatigue strength of the welded joints even if fine microstructure (e.g., small grain size, strong solid-solution strengthening, and higher dislocation density) is included in the joints. Gou et al. [33] welded joints in high-humidity environment to achieve different levels of porosity in the joints, and then tested the fatigue strength of the joints. They found that the fatigue resistance decreases with increasing in porosity. Similarly, Kar et al. [34] also reported that the reduction of porosity in the welded joint could enhance the fatigue strength since the pores can always promote the crack nucleation and thus decrease the fatigue strength. However, the effect of external reinforcement on the fatigue strength is much greater than the internal pores on the fatigue strength, as illustrated in Fig. 12, which may be due to the stronger notch effect produced by the reinforcement. This finding indicates that the joints should be grinded to be flat to have higher service life.

5 Conclusions

In this paper, AA6005 plates were welded via laser-arc welding technology under different welding parameters. The porosity, microstructure, and properties of the joints were examined. Based on the results and analysis above, the following conclusions are given:

(1) Macropores formed due to the instability of keyhole which could be well controlled by adjusting the welding parameters. Specifically, increasing arc currents and decreasing laser power could effectively reduce the porosity of the welded joints.

(2) The mechanism for reducing macropores was that the ratio of height-to-width of the keyhole was smaller when decreasing the laser power, which can prevent the keyhole from collapsing; increasing the arc currents can shorten the floating-up distance for the bubble to annihilate from the molten pool.

(3) By quantitative calculation, the mechanism for the formation of unavoidable micropores was found that the

solidification time (typical 8 ms) was too short for bubbles to float up to escape from the surface of the molten pool.

(4) EBSD results showed that the grain size of the fusion zone was about 74 ± 58 µm, and no obvious texture was found.

(5) The tensile testing results showed that the porosity had little influence on the tensile strength of welded joints when the porosity is in low range (near 0~4%), but the elongation was obviously affected by the porosity.

(6) Pores was found to be the main reason for the loss of fatigue strength of hybrid laser welded joints since the fatigue cracks preferred to initiate from the sites with pores close to the sample's surface.

References

1. Yan S, Nie Y, Zhu Z, Chen H, Gou G, Yu J, Wang G (2014) Characteristics of microstructure and fatigue resistance of hybrid fiber laser-MIG welded Al–Mg alloy joints. Appl Surf Sci 298: 12–18

2. Kutsuna M, Yan Q (1998) Study on porosity formation in laser welds in aluminium alloys Report 1 Effects of hydrogen and alloying elements. Weld Int 12:937–949

3. Zhang D, Li C, Liu X, Cao Y, Wu D (2018) Numerical study of spatter formation during fiber laser welding of aluminum alloy. J Manuf Process 31:72–79

4. Ki H, Mohanty PS, Mazumder J (2002) Modeling of laser keyhole welding part I. Mathematical modeling, numerical methodology, role of recoil pressure, multiple reflections, and free surface evolution. Metall Mater Trans A 33:1817–1830

5. Bunaziv I, Akselsen OM, Salminen A, Unt A (2016) Fiber laser-MIG hybrid welding of 5mm 5083 aluminum alloy. J Mater Process Technol 233:107–114

6. Texiera D, Atmania F, Bochera P, Nadeauc F, Chena J, Zedana Y, Vanderessea N, Demers V (2018) Fatigue performances of FSW and GMAW aluminum alloys welded joints: competition between microstructural and structural-contact-fretting crack initiation. Int J Fatigue 116:220–233

7. Wu SC, Yu C, Yu PS, Buffière JY, Helfen L, Fu YN (2016) Corner fatigue cracking behavior of hybrid laser AA7020 welds by synchrotron X-ray computed microtomography. Mater Sci Eng A 651: 604–614

8. Meng W, Li Z, Lu F, Wu Y, Chen J, Katayama S (2014) Porosity formation mechanism and its prevention in laser lap welding for T-joints. J Mater Process Technol 214(8):1658–1664

9. Sun J, Nie P, Lu F, Huang J, Feng K, Li Z, Guo B, Jiang E, Zhang W (2017) The characteristics and reduction of porosity in high-power laser welds of thick AISI 304 plate. Int J Adv Manuf Technol 93(9-12):3517–3530

10. Zhang C, Gao M, Wang D, Lin J, Zeng X (2017) Relationship between pool characteristic and weld porosity in laser arc hybrid welding of AA6082 aluminum alloy. J Mater Process Technol 240: 217–222

11. Katayama S, Yasuaki N, Satoru U, Masami M (2006) Physical phenomena and porosity prevention mechanism in laser-arc hybrid welding, transactions of JWRI 35, pp 13–18.

12. Leo P, Renna G, Casalino G, Olabi AG (2015) Effect of power distribution on the weld quality during hybrid laser welding of an Al–Mg alloy. Opt Laser Technol 73:118–126

13. Ola OT, Doern FE (2015) Keyhole-induced porosity in laser-arc hybrid laser welded aluminium. Int J Adv Manuf Technol 80:3–10

14. Casalino G, Mortello M, Leo P, Benyounis KY, Olabi AG (2014) Study on arc and laser powers in the hybrid welding of AA5754 Al-alloy. Mater Des 61:191–198

15. Yan S, Chen H, Ma C, Nie Y, Wang X, Qin QH (2015) Local corrosion behaviour of hybrid laser-MIG welded Al–Zn–Mg alloy joints. Mater Des 88:1353–1365

16. Yan S (2019) Multiscale study of the properties of hybrid laser-welded Al-Mg-Si alloy joints, Research Scool of Engineering, The Australia National University, p 27

17. Yan S, Xing B, Zhou H, Xiao Y, Qin Q-H, Chen H (2018) Effect of filling materials on the microstructure and properties of hybrid laser welded Al-Mg-Si alloys joints. Mater Charact 144:205–218

18. Atabaki MM, Ma J, Liu W, Kovacevic R (2015) Pore formation and its mitigation during hybrid laser/arc welding of advanced high strength steel. Mater Des 67:509–521

19. Chen M, Xin J, Xin L, Zhao Z, Wu F, Ma S, Zhang Y (2017) Effect of keyhole characteristics on porosity formation during pulsed laser-GTA hybrid welding of AZ31B magnesium alloy. Opt Lasers Eng 93:139–145

20. Panwisawas C, Perumal B, Ward RM, Turner N, Turner RP, Brooks JW, Basoalto HC (2017) Keyhole formation and thermal fluid flow-induced porosity during laser fusion welding in Ti alloys: Experiemtal and modelling. Acta Mater 126:251–263

21. Wu SC, Yu X, Zuo RZ, Zhang WH, Xie HL, Jiang JZ (2013) Porosity, element loss, and strength model on softening behavior of hybrid laser arc welded Al-Zn-Mg-Cu alloy with synchrotron radiation analysis. Weld Int 92:64–71

22. Kuryntsev SV (2019) Microstructure, mechanical and electrical properties of laser-welded overlap joint of CP Ti and AA2024. Opt Lasers Eng 112:77–86

23. Yan S, Zhou H, Qin QH (2019) Microstructure versus size nano microscale deformation of solute strengthening Al alloys via pillar compression tests. Mater Res Lett 7:53–59

24. Yan S, Chen H, Zhu Z, Gou G (2014) Hybrid laser-metal inert gas welding of Al–Mg–Si alloy joints: microstructure and mechanical properties. Mater Des 61:160–167

25. Lu F, Li X, Li Z, Tang X, Cui H (2015) Formation and influence mechanism of keyhole-induced porosity in deep-penetration laser welding based on 3D transient modeling. Int J Heat Mass Transf 90: 1143–1152

26. Madison JD, Aagesen LK, Chan VW, Thornton K (2014) Advancing quantitative description of porosity in autogenous laser-welds of 304L stainless steel. Integr Mater Manuf Innov 3: 11–28

27. Ribic B, Palmer TA, DebRoy T (2013) Problems and issues in laser-arc hybrid welding. Int Mater Rev 54(4):223–244

28. Seto N, Katayama S, Matsunawa A (2001) Porosity formation mechanism and suppression procedure in laser welding of aluminium alloys. Weld Int 15(3):191–202

29. Xiao R, Zhang X (2014) Problems and issues in laser beam welding of aluminum–lithium alloys. J Manuf Process 16(2):166–175

30. Seiji K, Yakacki N, Satoru U, Masami M (2006) Physical phenomena and porosity prevention mechanism in laser-arc hybrid welding. Trans JWRI 35:13–18

31. Wang Z, Oliveirac JP, Zeng Z, Bu X, Peng B, Shao X (2019) Laser beam oscillating welding of 5A06 aluminum alloys: microstructure, porosity and mechanical properties. Opt Laser Technol 11:58–65

32. Gao XL, Zhang LJ, Liu J, Zhang JX (2014) Porosity and micro-structure in pulsed Nd:YAG laser welded Ti6Al4V sheet. J Mater Process Technol 214:1316–1325

33. Gou G, Zhang M, Chen H, Chen J, Li P, Yang YP (2015) Effect of humidity on porosity, microstructure, and fatigue strength of A7N01S-T5 aluminum alloy welded joints in high-speed trains. Mater Des 85:309–317

34. Kar J, Chakrabarti D, Roy SK, Roy GG (2019) Beam oscillation, porosity formation and fatigue properties of electron beam welded Ti-6Al-4V alloy. J Mater Process Technol 266:165–172

Publisher's note Springer Nature remains neutral with regard to jurisdictional claims in published maps and institutional affiliations.